Concentration fluctuations in gas releases by industrial accidents

Nielsen, M.; Chatwin, P.C.; Ejsing Jørgensen, Hans; Mole, N.; Munro, R.J.; Ott, Søren

Publication date:
2002

Document Version
Publisher's PDF, also known as Version of record

COFIN project

Concentration Fluctuations in Gas Releases by Industrial Accidents

Final Summary Report

M. Nielsen, P.C. Chatwin, H. E. Jørgensen, N. Mole, R.J. Munro and S. Ott

Risø National Laboratory, Roskilde, Denmark
May 2002

Introduction

The EU-ENVIRONMENT project COFIN (ENV4-CT97-0629) is a relatively small project with two partners only – Risø National Laboratory and Sheffield University – who felt that the problem of concentration fluctuations had been given too little attention in the context of practical risk assessment. The main objective was *main objective*

> *to develop new models for the effects of random concentration fluctuations in hazardous gas releases*

and the method was to derive empirical relations from existing field data, in particular those obtained by the Risø Lidar. The purpose was to produce new theory and empirical relations for enhancement of operational models used for risk analysis.

Concentration fluctuations are usually ignored in risk assessment, probably because regulators consider currently available models too complex and difficult in application. It is our impression that consultants agree that a stochastic description could be a useful supplement, but their clients are reluctant to ask for analyses, which are not required in the regulation guidelines. The best way to improve the situation is probably to develop relatively simple model extensions compatible with the current standard.

With these objectives in mind, our main strategy for the COFIN project was to study existing field data and develop relevant relations by a combination of statistical analyses and appropriate surface-layer scaling. Our conceptual model for the process is a relatively narrow plume being swept from side to side by large eddies while mixed by turbulence comparable to or smaller than the plume dimension. The concentration fluctuations observed at a fixed point is the combined result of internal mixing and plume meandering. Plume meandering is a relatively slow process and the number of excursions within the duration of a typical experiment is not high. Therefore, cross-plume profiles of mean concentration or other statistics are surprisingly irregular and asymmetric when analysed in the fixed frame of reference. In contrast, profiles are smooth and reproducible when we analyse fluctuations in a moving frame of reference following the instantaneous plume centreline. *strategy*

Data

Data were selected from field experiments with continuous release of artificial smoke from sources near the ground. The experiments were conducted in several campaigns with similar set up in relatively homogeneous terrains free of obstacles. The measurements were made by a remote-sensing Lidar, which detects the smoke distribution along a laser beam. The wind and turbulence were monitored by meteorological equipment near the release point including at least one sonic-anemometer. The measuring path of the Lidar was oriented horizontally across the plume at approximately 1.5 m above terrain and the distances from the source were in the range 100-600 m, see figure 2. *field experiments*

In each measurement cycle the Lidar emits a short laser light pulse and detects the light reflected by smoke aerosols. The smoke concentration and distance from the instrument are deduced from the intensity and time-delay of the backscatter signal. Each Lidar profile contains 512 measuring range gates and the time response is practically instantaneous. Due to the dimensions of the light pulse and time response of the detector system, the virtual observation points have spatial averaging approximately 1.5 m along the laser beam. In the selected experiments the measuring frequency of the Lidar was $1/5 - 1/3$ Hz. For some analyses we apply additional data obtained a rebuilt Lidar, which has a faster measurement frequency, less measurement noise but more spatial averaging. We *Lidar*

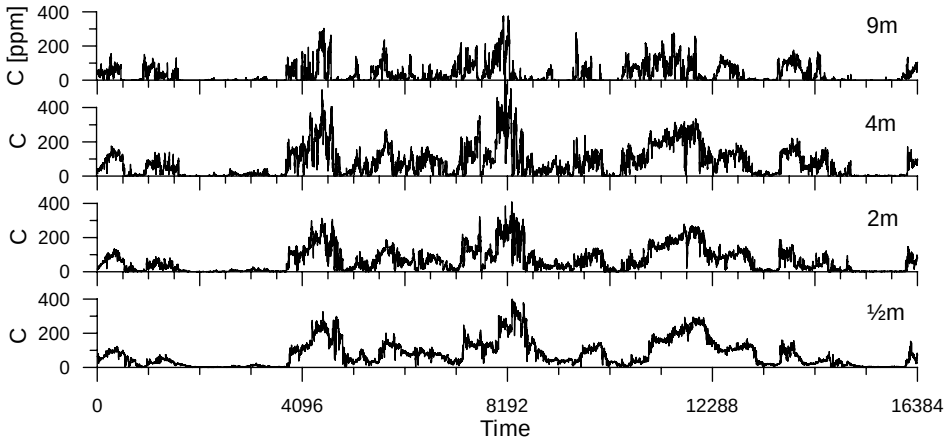

Figure 1. Time series measurements by UVIC sensors on a mast 235m downstream of a surface source – in the FLADIS experiments.

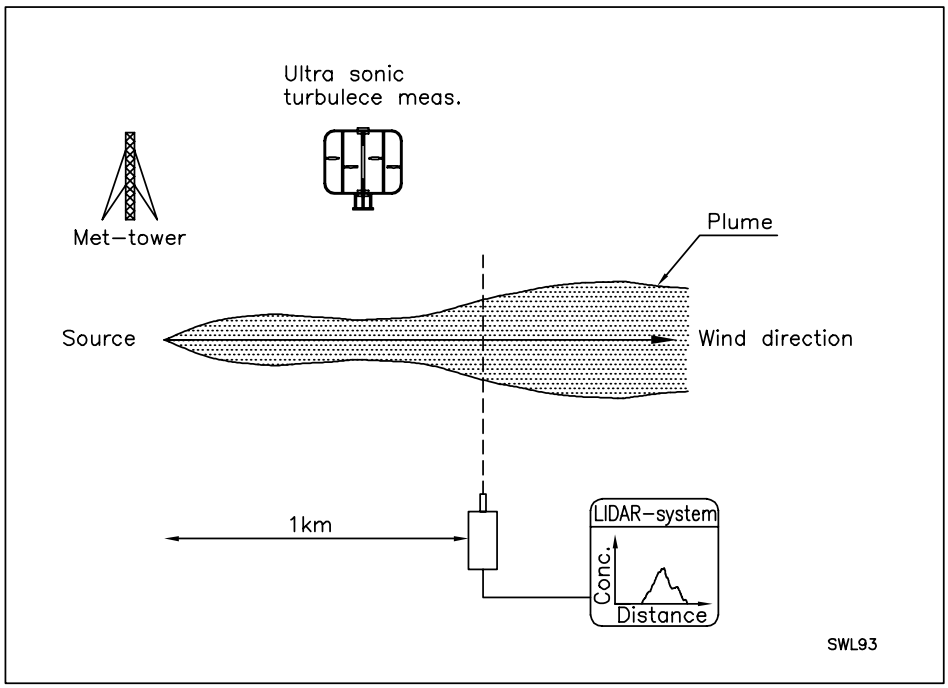

Figure 2. Top view of the typical setup of a lidar experiment.

also use data from the fast-responding UVIC detectors deployed at similar measurement positions.

data processing

The Lidar data are processed by an algorithm, which compensates for smoke obscuration and directional spreading of the reflected light. This algorithm uses a larger amplification and less ideal signal-to-noise ratios for smoke at far distance. The unsteady signal baseline is corrected by a curve fit through clean-air observation in front of and behind the plume, by a method which was refined during the COFIN project, see figure 3.

noise removal

Further signal improvement was obtained by a maximum-entropy-inversion (MEI) method, which reduces high-frequency noise while maintaining average and variance. This method is based on an assumption of uniform statistical properties, which is not fulfilled for a cross-plume profile. Instead we construct time-series at virtual observa-

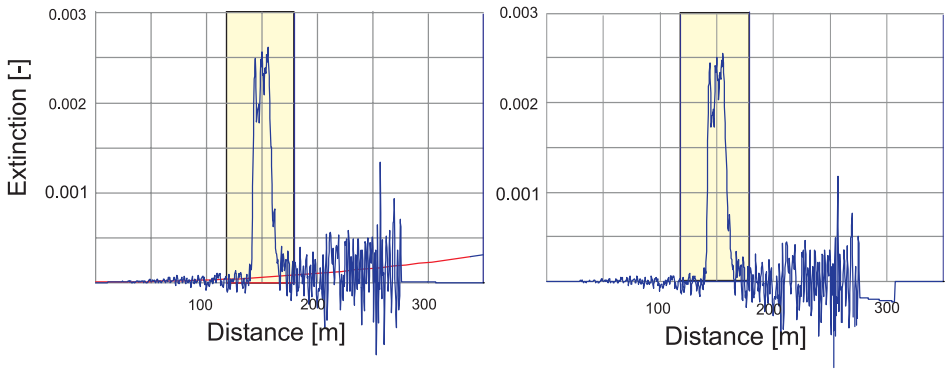

Figure 3. Example of a Lidar profile with and without baseline correction.

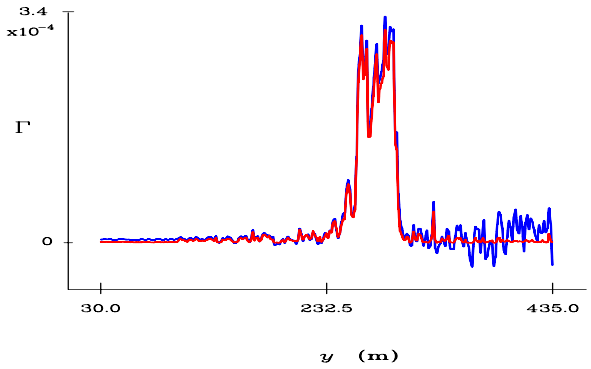

Figure 4. An instantaneous concentration profile, together with the same profile after application of the MEI procedure.

tion points and MEI treat these individually. This is a time consuming task difficult to automate and not all data were treated this way.

Analyses and models

versatile PDF model

The probability distribution function (PDF) is an important property of the concentration fluctuations. The Beta and generalized Pareto distribution (BGPD) is a very flexible PDF model, which is constructed as a weighted sum

$$p(c) = \gamma f_1(c) + (1-\gamma) f_2(c) \qquad 0 \le \gamma \le 1 \tag{1}$$

of two components

$$\begin{aligned} f_1(c) &= \frac{(1-c/c_{\max})^{\xi_2-1}}{\xi_1} & \xi_1 > 0, \xi_2 > 0 \\ f_2(c) &= \frac{(c/c_{\max})^{\eta_1}(1-c/c_{\max})^{\eta_2}}{c_{\max}\mathrm{B}(1+\eta_1,1+\eta_2)} & \eta_1 > -1, \eta_2 > 0 \end{aligned} \tag{2}$$

with the Beta function defined by $\mathrm{B}(m,n) \equiv \int_0^1 t^{m-1}(1-t)^{n-1}\,dt$. The BGPD model has five independent parameters $(\gamma, \xi_1, \xi_2, \eta_1, \eta_2)$ since the maximum concentration is determined by $c_{\max} = \xi_1\xi_2$. It will fit both uni- and bi-modal distributions, see figure 5, and its approach to the upper limit $p(c) \to \alpha(1-c/c_{\max})^{\beta}$ for $c \to c_{\max}$ is in agreement with UVIC data.

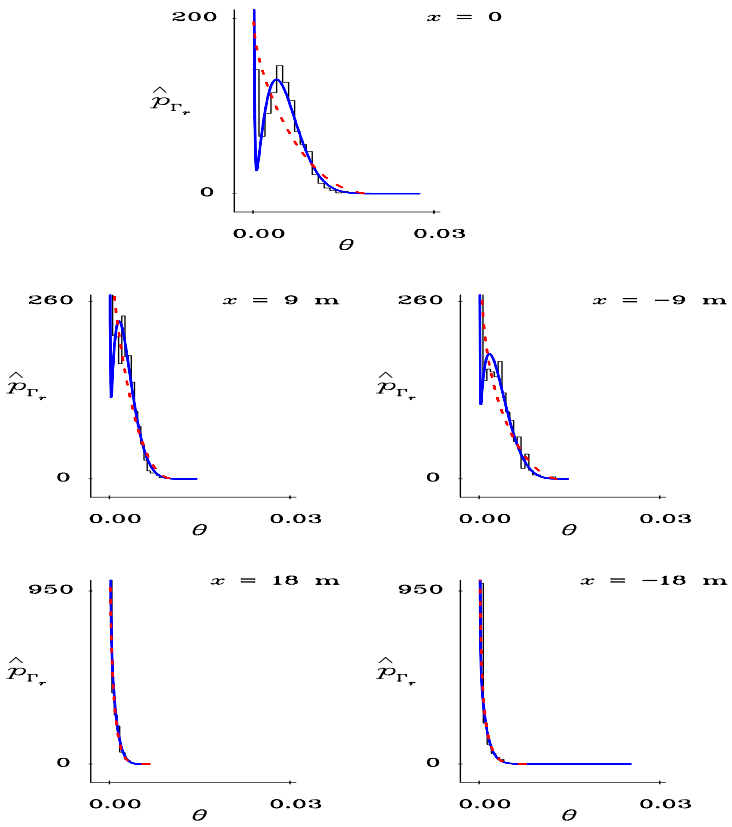

Figure 5. Maximum likelihood fits for the BGPD (solid curve), compared with the corresponding histogram, at moving-frame positions $x = 0$, $x = \pm 9\,m$ and $x = \pm 18\,m$, for the mad14k data. Also shown are the results of the maximum likelihood fits for the simpler beta distribution (dashed curve).

plume centreline

Lidar data offers an excellent opportunity to study spatial distribution of the concentration fluctuations. An important concept in our analyses is the plume centreline defined by

$$y_c\,(t) = \frac{1}{\hat{m}_1(t)} \int_{-\infty}^{\infty} y\, C\,(y,t)\, dy \tag{3}$$

where we normalize with a 'mass' integral of the type

$$\hat{m}_n(t) = \int_{-\infty}^{+\infty} C^n\,(y,t)\, dy \tag{4}$$

From this we define the moving-frame concentration

$$C_m\,(\xi,t) \equiv C\,(y_c\,(t) + \xi, t) \tag{5}$$

moving-frame profile

and the time-averaged moving-frame profile $\langle C_m\,(\xi,t)\rangle$. The shape of this profile, as well as for equivalent profiles for higher-order statistical moments $\langle C_m^{\,n}\,(\xi,t)\rangle$, is best described as gaussian near the centreline with exponential tails, see figure 6. Spatial dimensions of the moving-frame profiles is measured by

$$\sigma_n^2 \equiv \frac{\int_{-\infty}^{+\infty} \langle C_m^n\,(\xi,t)\rangle\, \xi^2 d\xi}{\langle \hat{m}_n\,(t)\rangle} \tag{6}$$

and we find, see figure 7, that these dimensions are interrelated by

$$\sigma_1/\sigma_n = (n+\beta)/(1+\beta) \quad \text{with} \quad \beta \simeq 2 \tag{7}$$

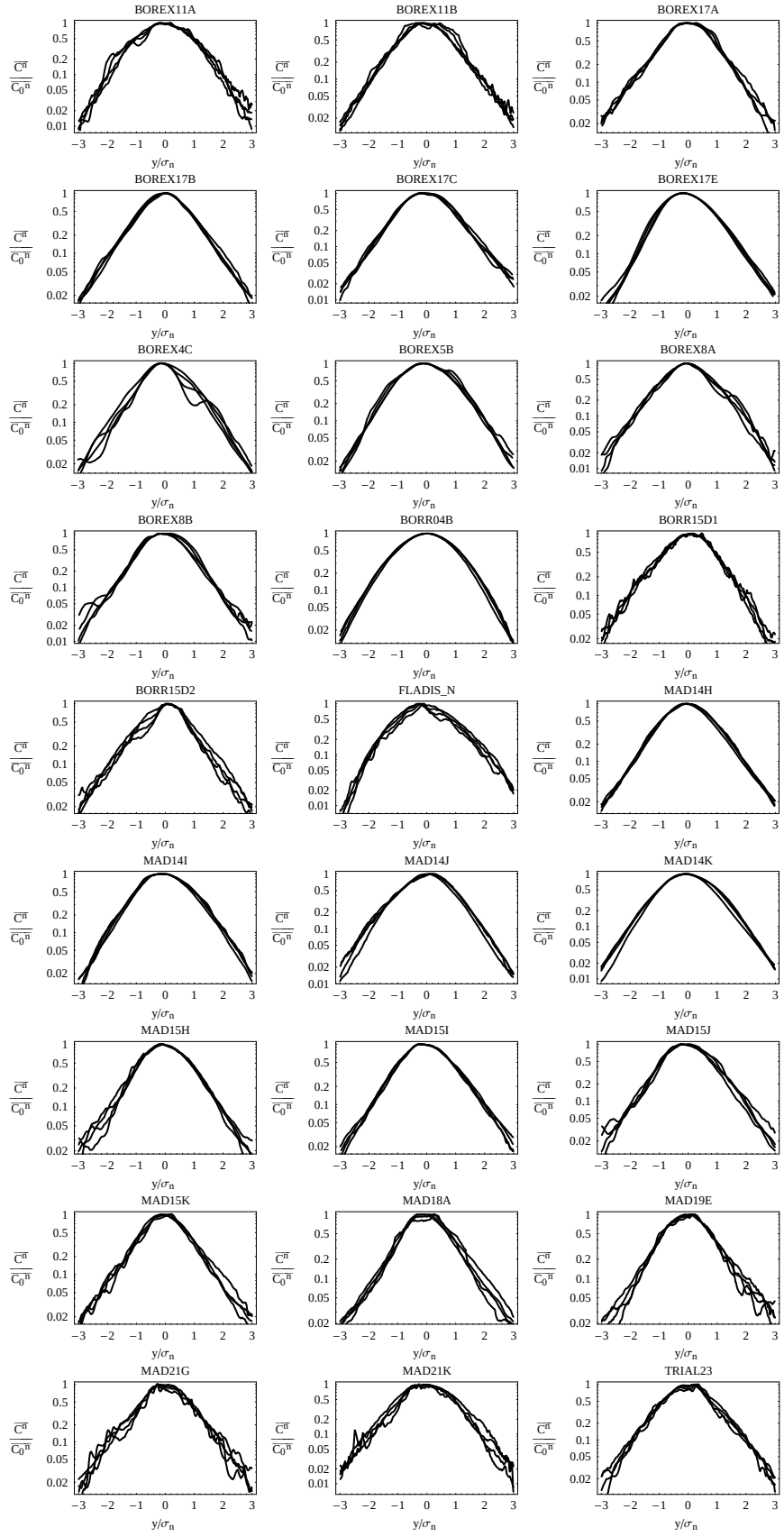

Figure 6. Normalized moment profiles for several ground releases, shown for $n = 1..4$

Thus, we may use σ_1 as a single characteristic length scale, and data shows that this is proportional to the friction velocity u_* and travel time t from the source, with the best estimate $\sigma_1 \simeq 0.75 u_* t$. No dependence on other meteorological parameters, such as atmospheric stability z/L, was detected.

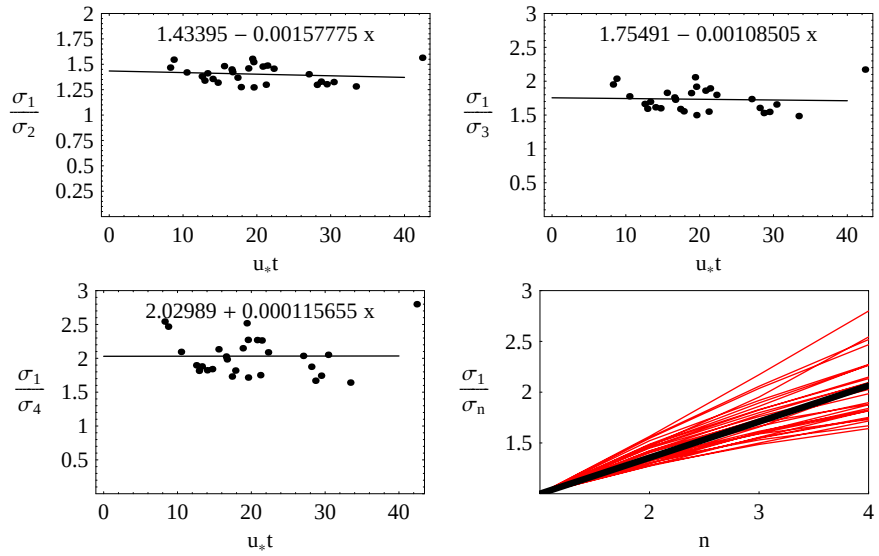

Figure 7. The ratios of σ_1/σ_n for n=2,3 and 4 shown as functions of $u_* t$. The plot in the lower right corner shows σ_1/σ_n vs. n. The thick line is equation 7 with $\beta = 1.88$

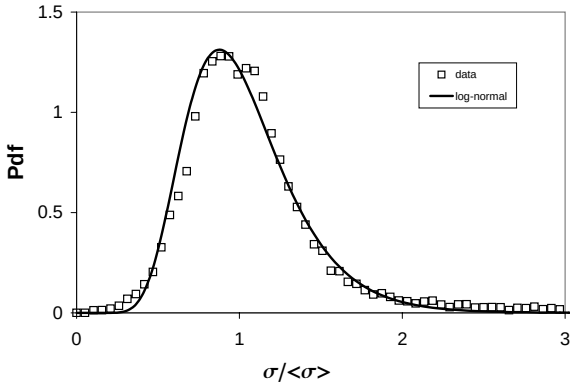

Figure 8. Plume width pdf based on all experiments. The line is a log-normal distribution with $b_\sigma = 0.32$.

The instantaneous plume width is defined by *instantaneous plume width*

$$\hat{\sigma}_n^2(t) \equiv \frac{\int_{-\infty}^{+\infty} C_m^n(\xi,t)\,\xi^2 d\xi}{\hat{m}_n(t)} \tag{8}$$

and the probability distribution of this is found to be log-normal, see figure 8 . Variation of the normalizing integral $\hat{m}_n(t)$ are modest and this definition is in reasonable agreement with the previous one $\langle \hat{\sigma}_n^2(t) \rangle \approx \sigma_n^2$.

In search for an explanation of the non-gaussian moving-frame profiles we describe *non-gaussian profiles* the development of the moving-frame profile by a diffusion equation

$$\frac{dC_m(\xi,t)}{dt} = \frac{d}{d\xi} K(\xi,t) \frac{dC_m(\xi,t)}{d\xi} \tag{9}$$

This follows from the assumption of self-similarity and by appropriate scaling the special diffusivity and moving-frame concentration profiles may be expressed by

$$K(\xi,t) = \sigma\dot{\sigma}\Phi(\xi/\sigma) \quad \text{and} \quad C_m(\xi,t) = \sigma^{-1}\mathrm{f}(\xi/\sigma) \tag{10}$$

and insertion into the above diffusion equation provides the relation

$$\mathrm{f}(s) \propto \exp\left[-\int_0^s s'/\Phi(s')\,ds'\right] \quad \text{with } s = \xi/\sigma \tag{11}$$

Further assumptions on diffusivities at small and large separations suggest the diffusivity profile $\Phi(s) = \frac{1}{4}(1+2|s|)$ producing a concentration profile

$$\mathrm{f}(s) = \tfrac{1}{2}(1+2s)\exp(-2s) \tag{12}$$

which indeed is nearly gaussian for small separations and exponential for large ones. Alternatively we might choose the more flexible formulation $\Phi(s) = (\alpha\beta)^{-2}\sqrt{1+(\beta s)^2}$ which leads to

$$\mathrm{f}(s) = \exp\left(-\alpha^2\left(\sqrt{1+\beta^2 s^2}-1\right)\right) \tag{13}$$

where $K_n(x)$ is the modified Bessel function of the second kind and where we set $\beta^2 = K_2(\alpha^2)\left[\alpha^2 K_1(\alpha^2)\right]^{-1}$ in order to match the plume width. This shape is gaussian for $\alpha \to \infty$, exponential for $\alpha \to 0$ and in agreement with equation 12 for $\alpha \approx 1$. The method could be used for other dispersion processes than in the selected experiments, e.g. an elevated plume which obeys different scaling laws. We hope to verify such predictions by future experiments.

time averaging

Historically, many tracer experiments have applied arrays of bag samples detecting the average concentration over the sample time t_s. Defining the normalized concentration $\int c(y,t)dy = 1$ we find the time average

$$\bar{c} = \frac{1}{t_s}\int_{t_0}^{t_0+t_s} c(y,t)\,dt \tag{14}$$

The meandering plume centreline implies that a plume width based on time-averaged measurements is wider that the instantaneous width. This is expressed as

$$\left\langle\sigma^2(t_s)\right\rangle = \left\langle\sigma^2(0)\right\rangle + \frac{1}{t_s^2}\int_0^{t_s}(t_s-\tau)S(\tau)\,d\tau \tag{15}$$

using a structure function for the centre-line position $S(\tau) = \left\langle\left(y(t+\tau)-y(t)\right)^2\right\rangle$.

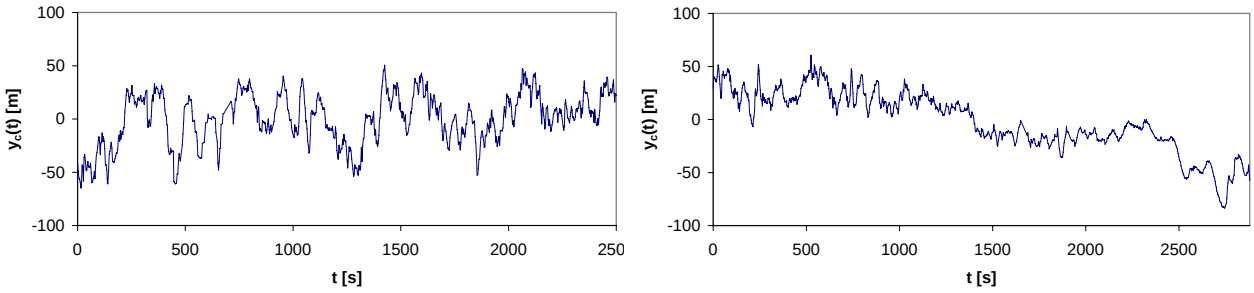

Figure 9. Plume centre as a function of time. Left: BOREX4c. Right: BOREX17E.

plume meander

The Langevin process is a suitably simple model for the centreline position

$$\frac{dy_c}{dt} = -\frac{y_c}{T} + U \cdot a\,(s) \tag{16}$$

with $s = tU/\sigma\,(0)$ and $\langle a\,(s')\,a\,(s'')\rangle = \lambda\delta\,(s'-s'')$ where T is a timescale, U is the plume advection, and a is a random memoryless gaussian acceleration. The variance and structure function become $\left\langle y_c^2\right\rangle = \frac{1}{2}\lambda\sigma\,(0)\,UT$ and $S\,(\tau) = \lambda\sigma\,(0)\,UT\,[1-\exp\,(-\tau/T)]$ Fitting this model to data is complicated by the frequently observed non-stationary plume meander, which is the fundamental difficulty of fixed-frame analyses, see right-hand frame of figure 9. With this reservation in mind, we propose $UT/\sigma\,(0) \simeq 30$ and $\lambda \simeq 0.2$. The Langevin process leads to the time-averaged plume width

$$\sigma^2\,(t) = \sigma^2\,(0) + \frac{\lambda\sigma\,(0)\,UT^3}{t^2}\left(1 - t/T + \tfrac{1}{2}\,(t/T)^2 - e^{-t/T}\right) \tag{17}$$

which is a useful formula when comparing different experiments using varying sample times. A further consequence of the Langevin-type plume meander model, is that the probability distribution of centre-line positions at two distinct times becomes joint gaussian with exponentially decaying correlation, i.e.

$$p\,(y_c', y_c'') = \frac{1}{2\pi\,\langle y_c^2\rangle\left(1-e^{-2|\tau|/T}\right)}\exp\left[-\frac{(y_c')^2 + (y_c'')^2 - 2y_c'y_c''e^{-|\tau|/T}}{2\,\langle y_c^2\rangle\left(1-e^{-2|\tau|/T}\right)}\right] \tag{18}$$

where we write $y_c' = y_c\,(t)$ and $y_c'' = y_c\,(t+\tau)$.

moving-frame PDF

We have developed methods for prediction of concentration-fluctuation PDF in a moving frame of reference. For this purpose we apply generic probability models of the type

$$p\,(c\,|\xi\,) = (1-\gamma\,(\xi))\,\delta\,(c) + \gamma\,(\xi)\,p_c\,(c\,|\xi\,) \tag{19}$$

where the intermittency $\gamma\,(\xi)$ is the probability of non-zero concentrations and $p_{\,c}\,(c\,|\xi\,)$ is a conditional PDF. Statistical moments of various statistical orders are linked to the PDF by

$$\langle C_m^n\,(\xi,t)\rangle = \int_0^\infty p\,(c\,|\xi\,)\,c^n dc \tag{20}$$

The spatial variation of these has a universal shape of the moving-frame profiles $f\,(\xi/\sigma_{\,n}) = \langle C_m^n\,(\xi,t)\rangle/\langle C_m^n\,(0,t)\rangle$ and spatial dimensions σ_n, which we prescribe by equations 12 and 7. With an empirical centre-line PDF of the form

$$p\,(c\,|0\,) = 4c/c_0^2\exp\,[-2c/c_0] \tag{21}$$

and the use of a generating function, we predict a general PDF by

$$p\,(c\,|\xi\,) = \frac{4c\exp\left[-2c/c_0e^{2s} + 2s\,(3-\beta)\right]}{c_0^2}\,\frac{1+2s\left(\beta-2+2c/c_0e^{2s}\right)}{1+2\beta s} \tag{22}$$

where $s = |\xi|/(\sigma_1 + \beta\sigma_1)$ is the dimensionless distance from the centreline. The fluctuation intermittency is interpreted as the zero order statistics

$$\gamma\,(\xi) = (1+2\,|\xi|/\sigma_0)\exp\,(-2\,|\xi|/\sigma_0) \tag{23}$$

with σ_0 determined by equation 7. This PDF model is in good agreement with empirical probability distributions, see figure 10.

An alternative strategy is to derive local PDFs by local statistical moments, e.g. from the gamma distribution

$$p\,(c) = (1-\gamma)\,\delta\,(c) + \frac{\gamma c^{b-1}}{\Gamma\,(b)\,a^b}\exp\,(-c/a) \Rightarrow \langle C^n\rangle = \gamma a^n\frac{\Gamma\,(n+b)}{\Gamma\,(b)} \tag{24}$$

The model coefficients are deduced from statistical moments

$$b = \frac{2-M_3}{M_3-1} \quad a = \frac{M_2}{1+b}\,\langle C\rangle \quad \gamma = \frac{1}{ab}\,\langle C\rangle \tag{25}$$

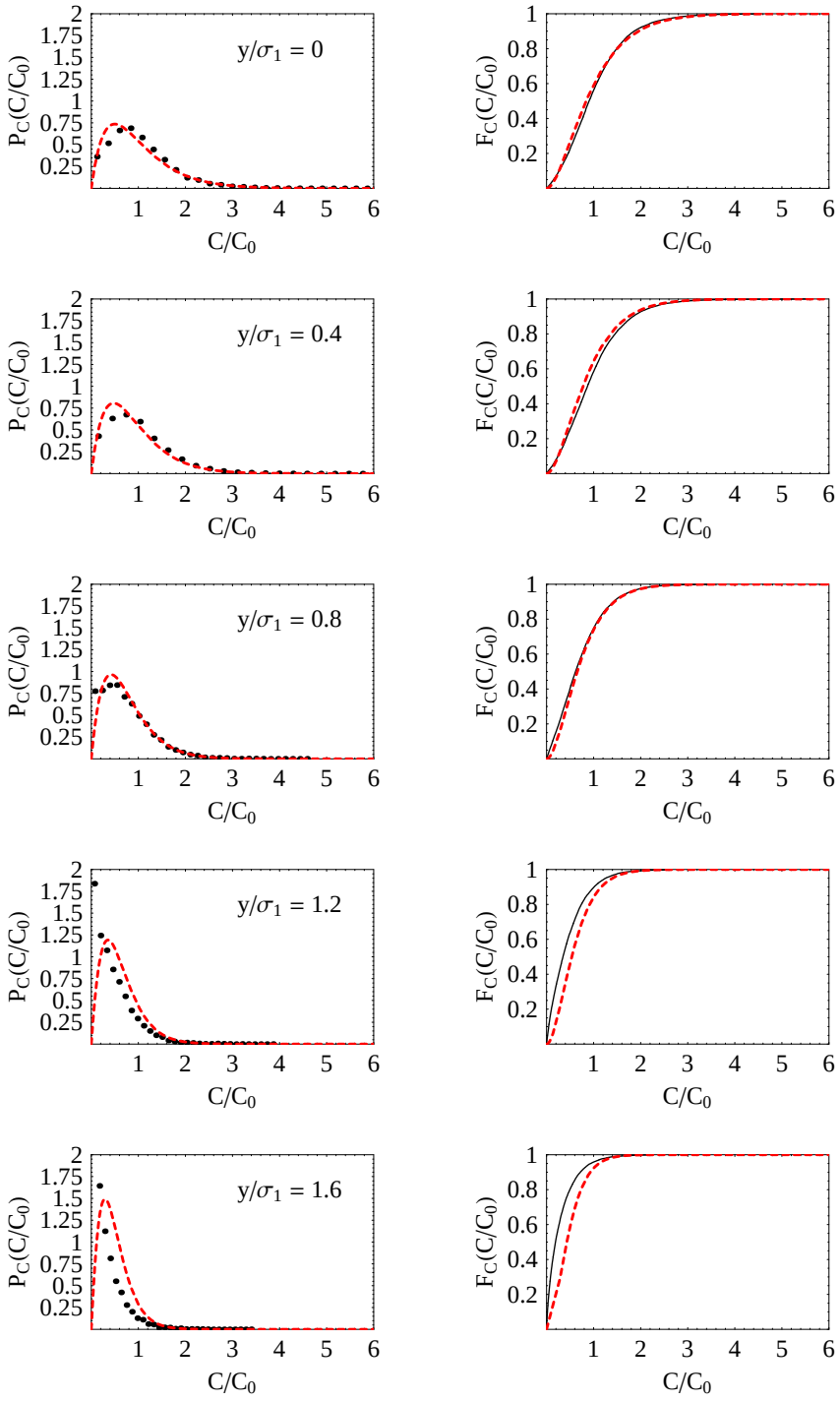

Figure 10. Conditional moving frame pdfs and cdfs for different values of $|y|/\sigma_1$. Points are data and the line is the proposed model.

using dimensionless moment ratios

$$M_2 = \frac{\langle C^2 \rangle}{\langle C \rangle^2} \quad M_3 = \frac{\langle C^3 \rangle \langle C \rangle}{\langle C^2 \rangle^2} \quad \text{and} \quad M_4 = \frac{\langle C^4 \rangle \langle C \rangle}{\langle C^3 \rangle \langle C^2 \rangle} \tag{26}$$

The shape parameter b of the gamma distribution must be positive, so solutions only exist for $1 \leq M_3 \leq 2$. Other PDF models, e.g. a clipped Gaussian distribution, impose similar

restrictions. Furthermore, observed profiles of moment ratios are concave with $M_n''(O) \approx \mathrm{O}(0.1)$. From these conditions we calibrate the parameters (α_n, σ_n) in moving-frame profiles of the type in equation 13

$$\langle C_m^n(\xi)\rangle = \langle C_m^n(0)\rangle \exp\left[-\alpha_n^2\left(\sqrt{1+\frac{K_2(\alpha_n^2)\,\xi^2}{\alpha_n^2 K_1(\alpha_n^2)\,\sigma_n^2}}-1\right)\right] \tag{27}$$

Profile dimensions deduced by this method are in good agreement with equation 7.

fixed-frame PDF

Fixed-frame probabilities and statistical moments are predicted by the convolution of the PDF for the centre-line position and the moving-frame statistics

$$\begin{aligned} p(c\,|y) &= \int_{-\infty}^{\infty} p(y_c)\, p_m(c\,|y-y_c)\,dy_c \\ \langle C^n(y)\rangle &= \int_{-\infty}^{\infty} p(y_c)\,\langle C_m^n(y-y_c)\rangle\,dy_c \end{aligned} \tag{28}$$

With a gaussian distribution of the centreline position and numerical integration the fixed-frame distributions of statistical moments follow nearly the same model as moving-frame distributions, however with wider distributions, smaller centreline values and more gaussian distributions, i.e. a larger fixed-frame tail parameter $\alpha_{n,f} > \alpha_{n,m}$. The fixed-frame moments at the centreline are found analytically for special moving-frame shapes ($\alpha_{n,m} = 0, 1, \infty$) and interpolated for the general case. Further conditions on tail behaviour and conservation of the moment integral determines the remaining fixed-frame parameters $(\alpha_{n,f}, \sigma_{n,f})$.

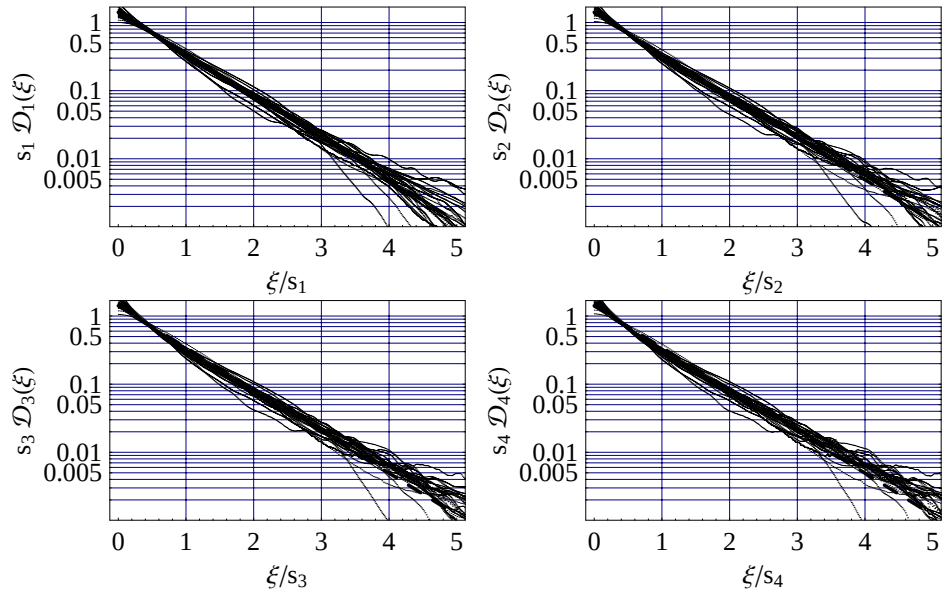

Figure 11. Generalized distance neighbour functions for $n = 1..4$.

distance-neighbour function

As a supplement to the moving-frame analyses we propose a generalized distance-neighbour function defined by

$$D_n(\xi) \equiv \int_{-\infty}^{+\infty} \left\langle \frac{C(y,t)\,C^n(y+\xi,t)}{\hat{m}_1(t)\hat{m}_n(t)} \right\rangle dy \tag{29}$$

This statistics describes the concentration structure around a randomly chosen plume particle. Similarly to the moving-frame profiles we define the width of the distance-

neighbour

$$s_n^2 \equiv \int_{-\infty}^{+\infty} D_n(\xi)\,\xi^2 d\xi \tag{30}$$

and the definitions leads to a nice relation between distance-neighbour and moving-frame dimensions.

$$s_n^2 = \langle \hat{\sigma}_1^2 \rangle + \langle \hat{\sigma}_n^2 \rangle \tag{31}$$

We also have the formula

$$\int_{-\infty}^{+\infty} D_1(\xi)\,\xi^4 d\xi = 2\int_{-\infty}^{+\infty} \frac{\langle C_m(\xi)\rangle\,\xi^4 d\xi}{\langle m_1(t)\rangle} + 6\langle \hat{\sigma}^4 \rangle \tag{32}$$

where the last term is related to the variance of the square of the instantaneous plume width. Data shows that the shape of the distance-neighbours is exponential, see figure 11 and by the definitions we obtain

$$D_n(\xi) = \frac{1}{\sqrt{2}\,s_n} \exp\left(-\sqrt{2}|\xi|/s_n\right) \tag{33}$$

which is equal to $D_1(\xi) = (2\sigma_1)^{-1}\exp(-|\xi|/\sigma_1)$ for the lowest order.

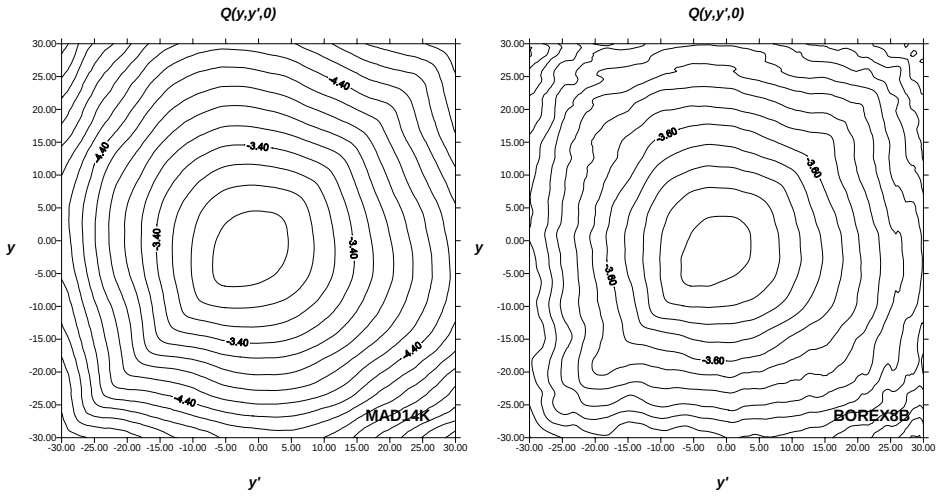

Figure 12. Contour plots of $Q(y, y', 0)$ made for two experiments. The contour levels are on a logarithmic scale with five contours per decade.

The time-lagged two-point correlation is defined by *two-point correlation*

$$Q(y, y', \tau) \equiv \langle C_m(y, t+\tau)\, C_m(y', t)\rangle \tag{34}$$

Data shows that this becomes

$$Q(y, y', 0) \approx \frac{1}{2\sigma_1^2} \exp\left[-\frac{|y+y'| + |y-y'|}{\sigma_1}\right] \tag{35}$$

for zero time lag, see figure 12, which is in accordance with the simple model for the moving-frame profile in equation 12. The concentrations become independent for larger time lags

$$Q(y, y', \tau) \to \langle C_m(y)\rangle \langle C_m(y')\rangle \quad \text{for} \quad \tau \to \infty \tag{36}$$

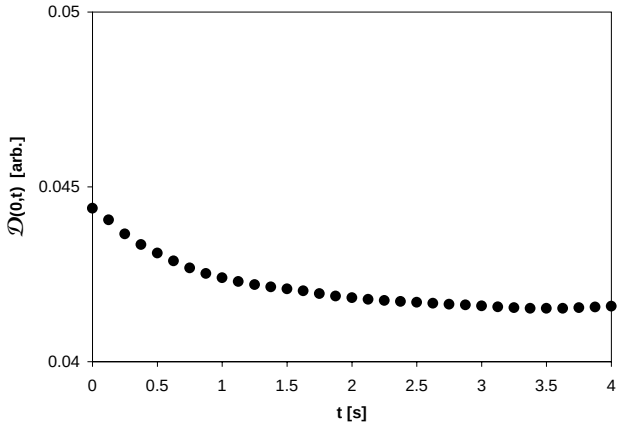

Figure 13. $\mathcal{D}(0,\tau)$ vs τ. PORTON data.

and actually this happens very fast, i.e. the in-plume fluctuations have a short memory, see figure 13. From the two-point correlation we may define a time-lagged distance-neighbour function

$$D\left(\xi,\tau\right) \equiv \int_{-\infty}^{\infty} Q\left(\xi+y,y,\tau\right) dy \tag{37}$$

as an extension to the previous definition for $D\left(\xi\right) = D\left(\xi,0\right)$. From new fast Lidar data we find an exponential decay of the zero-separation case $D\left(0,\tau\right)$ with a time constant less than one second. We may also define a similar quantity

$$\varepsilon\left(\xi,\tau\right) \equiv \int_{-\infty}^{\infty} Q\left(\xi-y,y,\tau\right) dy \tag{38}$$

and data shows that for zero time lag we may use the separation

$$Q\left(y,y',0\right) \approx 2D\left(\left|y-y'\right|,0\right)\varepsilon\left(\left|y+y'\right|,0\right) \tag{39}$$

Simulation tools

The aim of simulation is to produce artificial 'signals', which might substitute real data as input to consequence models or simply illustrate the process. For a simulation to be of interest the statistical properties of the 'signals' must be realistic, i.e. it should reproduce as many statistical parameters as possible. Perfect imitation is impossible, although the available methods may reproduce the PDF of individual time series and second-order accurate cross-correlations of time series pairs. The statistics of the time-derivatives of the signals are modelled correctly to the second order.

Fourier simulation of gaussian processes

Simulation of random processes is greatly simplified when the target probability functions are gaussian. The main advantage is that a linear transformation of a vector y_j with gaussian components will map into another gaussian vector $x_i = L_{ij}y_j$, where L_{ij} is the transformation matrix. If the input variables y_j are uncorrelated gaussian deviates, simulated by the Box-Muller algorithm (Press, Flannery, Teukolsky & Vetterling 1992), the covariance matrix of the transformed process is $K = LL^T$, where L^T is the transposed of the covariance matrix. Simulation by $x_i = L_{ij}y_j$ is called Karhunen-Loève expansion. Proper covariance matrices always non-negative definite and the transformation matrix

L may be found by Cholesky, or 'square root', decomposition of the covariance matrix (Press et al. 1992). Another useful property is that a Fast Fourier Transform (FFT) of a Gaussian time series maps onto a gaussian spectral distribution, and vice versa. Spectral representations $X_i(f)$ and $X_j(f)$ the time series $x_i(t)$ and $x_j(t)$ may be modelled by uncorrelated gaussian input $X_i(f) = L_{ik}(f) Y_k(f)$ and transformed into time domain by inverse FFT. The starting point for numerical simulation is the cross spectrum matrix, which is decomposed for every frequency, $\chi_{ij}(f) = L(f) L^*(f)$. In general, we must use complex algebra since cross-correlation functions may be asymmetric in time with corresponding complex cross spectra. The spectral matrix will be Hermitian $\chi_{ij}(f) = \chi^*_{ij}(f)$, and the non-negative definiteness allows decomposition by a complex version of the Cholesky's algorithm.

non-gaussian simulation by iteration

Many techniques for simulation of non-gaussian variable applies a memoryless translation, in which the individual series $x_i(t)$ is transformed by the monotonic increasing function $c_i(t) = g_i[x_i(t)] = F^{-1}_{C_i}[\phi_{X_i}[x_i(t)]]$, where F_{C_i} is the marginal distribution of $c_i(t)$ and ϕ_{X_i} is the distribution of the preliminary series. The difficulty of this procedure is that the transformation distorts the spectral distribution. The first method tested in COFIN applied an iteration, which alternately corrects the PDF and the spectral distribution of the series. In each iteration step, we find the distribution of the preliminary series $= F^{-1}_{C_i}[\phi_{X_i}[x_i(t)]]$ by the QUICKSORT algorithm. The spectral corrections are made by

$$\chi_{i+1}(f) = \frac{\chi_i(f)}{\chi_i^{\mathrm{map}}(f)} \chi_i^{\mathrm{T}}(f) \tag{40}$$

where $\chi_{i,k}(f)$ and $\tilde{\chi}_{i,k}(f)$ are the power spectra of the preliminary series and corresponding probability corrected one and $\chi_{i,T}(f)$ is the target power spectrum. The iteration is stopped when corrections are sufficiently small. The method also applies for uniform two- or multidimensional fields using corresponding versions of the FFT algorithm. Useful simulations were obtained by relaxation of the requirement of uniformity. A two-dimensional simulation was made in domain of time and cross-plume position with the probability correction depending on cross-plume position. From a theoretical viewpoint this method is inaccurate, since the spectral distortion by the probability correction vary with plume position whereas spectral corrections are universal.

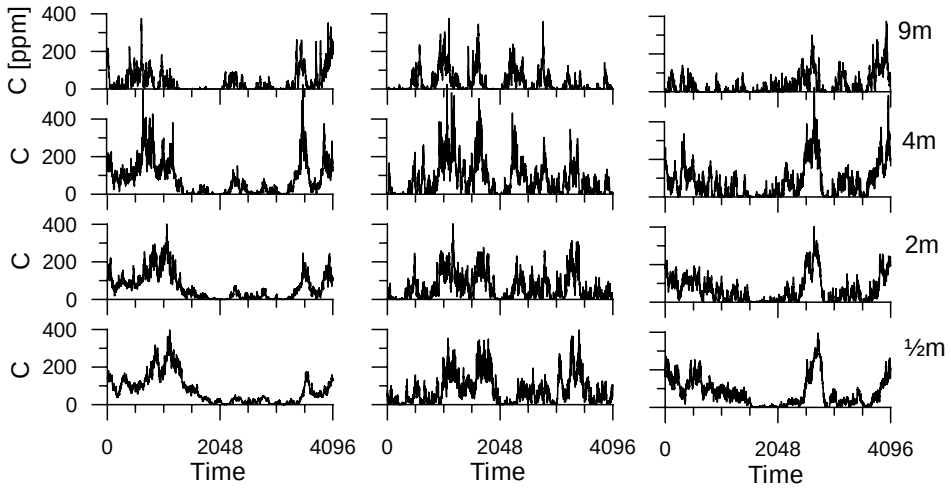

Figure 14. Time series simulated by the correlation-distortion method and imitating the FLADIS measurements shown in figure 1.

correlation-distortion

Correlation-distortion is a simulation method in which the spectral distributions used for Fourier simulation are modified such that the subsequent probability correction will results in the target spectra. This is efficient since no iteration is required. Gioffrè, Gusella

& Grigoriu (2000) show that for a given time lag τ the cross correlation function of the two translated processes $\rho_{c_i c_j}(\tau)$ relates to the cross correlation of the initial series $\rho_{x_i x_j}(\tau)$ by a double integral involving the translation functions.

$$\sigma_{C_k}\sigma_{C_l}\xi_{kl}(\tau) = \int_{-\infty}^{\infty}\int_{-\infty}^{\infty}[g_k\{x_k\}-\mu_k][g_l\{x_l\}-\mu_l]\,\varphi_{2\mathrm{D}}[x_k, x_l\,|\rho_{kl}(\tau)]\,dx_k\,dx_l \tag{41}$$

Here $\mu_k = \mathrm{E}[c_k]$ is the mean of the non-gaussian process and $\varphi_{2\mathrm{D}}$ is the joint gaussian distribution. The task is to find correlation functions for the gaussian processes $\rho_{x_i x_j}(\tau)$, which will reproduces the target correlations for the non-gaussian processes $\rho_{c_i c_j}(\tau)$. Numerical evaluation of the double integral is computationally expensive and a solution is needed for all signal pairs. To speed up the calculations we apply a Taylor expansion

$$\sigma_k\sigma_l\xi_{kl}(\tau) \approx \sum_{n=1}^{N}\frac{a_{kn}a_{ln}}{n!}\rho_{kl}^n(\tau) \tag{42}$$

with coefficients $a_{kn} = \int[g_k\{x\}-\mu_k]\,He_n(x)\,\phi(x)\,dx$ calculated by Hermite polynomials $He_n(x) \equiv (-1)^n\,\mathrm{D}^n[\varphi(x)]/\varphi(x)$ defined by the normal distribution $\varphi(x)$. The cross-correlations of all combinations of gaussian processes $\rho_{x_i x_j}(\tau)$ are transformed to the frequency-dependent cross-spectral matrix $\rho_{x_i x_j}(\tau)$ and used for Fourier simulation of gaussian series, which are translated to non-gaussian ones $c_i(t) = g_i[x_i(t)]$. Unfortunately, lack of precision in the Taylor expansion and Fourier transformation will sometimes corrupt the positive definiteness of the translated correlation matrices. To overcome this problem we decompose spectral matrices by an alternative eigensystem method and adopt a special correction, which recovers positive definiteness of the correlation matrix with minimum adjustment of cross correlations and conservation of autocorrelations. Figure 14 shows simulations by this method.

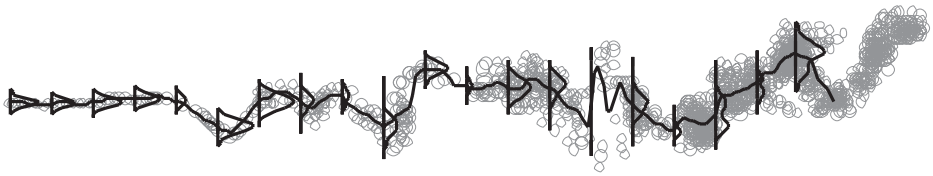

Figure 15. Snapshot of a plume-meander simulation.

plume meander

A random 2-D turbulence-like velocity field is simulated by a single length constant and an eddy lifetime modelled by the wave number $T \propto |k|^{-2/3}$. Gaussian puffs are released from the source and tracked in the time-varying flow field. The puff grows linearly in time until they reach a predefined size after which they split into three smaller ones with their masses and weighs designed for a match with the first four spatial moments of the mother puff. The total concentration field is determined as the sum of all traces determined as cubic-spline interpolations through series of gaussian puffs. The moments of the composite concentration field is measured as sums of the well-known moments of gaussian distributions, and from this we determine the centre-line position and plume width as function of time and downwind position, see figure 15.

Sometimes we only need to simulate plume meander at a single downwind position, and for these cases it is much simple to use the Langevin equation 16, which implies that the plume position after time step Δt has a normal distribution

$$p(y_c(t+\Delta t)\,|y_c(t)) \in \mathrm{N}\left(\alpha y_c(t), \left(1-\alpha^2\right)\left\langle y_c^2\right\rangle\right) \tag{43}$$

depending on the total variance $\langle y_c^2 \rangle$ and the exponentially decaying 'memory' $\alpha = \exp(-\Delta t/T)$ of the temporal position $y_c(t)$.

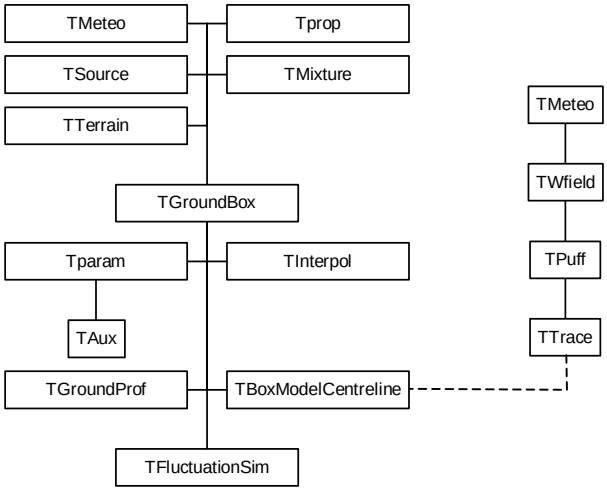

Figure 16. Structure of the COFINBOX model.

Demonstration software

heavy-gas model

It was decided to develop a computer program COFINBOX, which demonstrates that models for concentration fluctuations might be used as an add-on module for traditional dispersion models. For this purpose we implement a heavy-gas box model, which is a model type often used in risk assessment. The program is modular with objects for: meteorological conditions; phase-transition and density calculations for two-phase mixtures with aerosols in homogeneous equilibrium; simple source models determining the release conditions; main parameters used for integration (enthalpy, width, mass, momentum and position); auxiliary parameters derived by the main parameters (concentration, temperature, density, turbulence velocity scales, etc.); fourth-order Runge-Kutta integration of ordinary differential equations for main parameters with adaptive time steps; smooth interpolation between main parameters. Mixing is predicted by a heavy-gas entrainment function based on estimates for in-plume friction velocity and heat flux from the ground, with a smooth transition from heavy-gas to passive dispersion. The model structure is shown in figure 16.

concentration fluctuations

These calculations are standard in box models for heavy-gas dispersion. The objects for concentration fluctuations are: probability and simulation of the plume centreline position using a Langevin equation; prediction of moving-frame profiles for various statistical moments; and simulation of concentration fluctuation. The simulation is based on iteration in a two-dimensional time/cross-plume direction domain using a simple model for the spectral structure. The ideal simulation technique would be distortion-correlation of coupled time series, but we have not yet found a model for spectral coherence of fluctuations in a meandering plume observed on a fixed frame of reference.

kinematic simulation

The computationally efficient Langevin-equation method for local plume meander substitutes an elaborated kinematic simulation. Although no longer needed for simulation of concentration fluctuations, the kinematic simulation is maintained as an illustration of the plume meander process. This simulation is driven by a random two-dimensional horizontal velocity field with a wave-number dependent memory making lifetimes of large

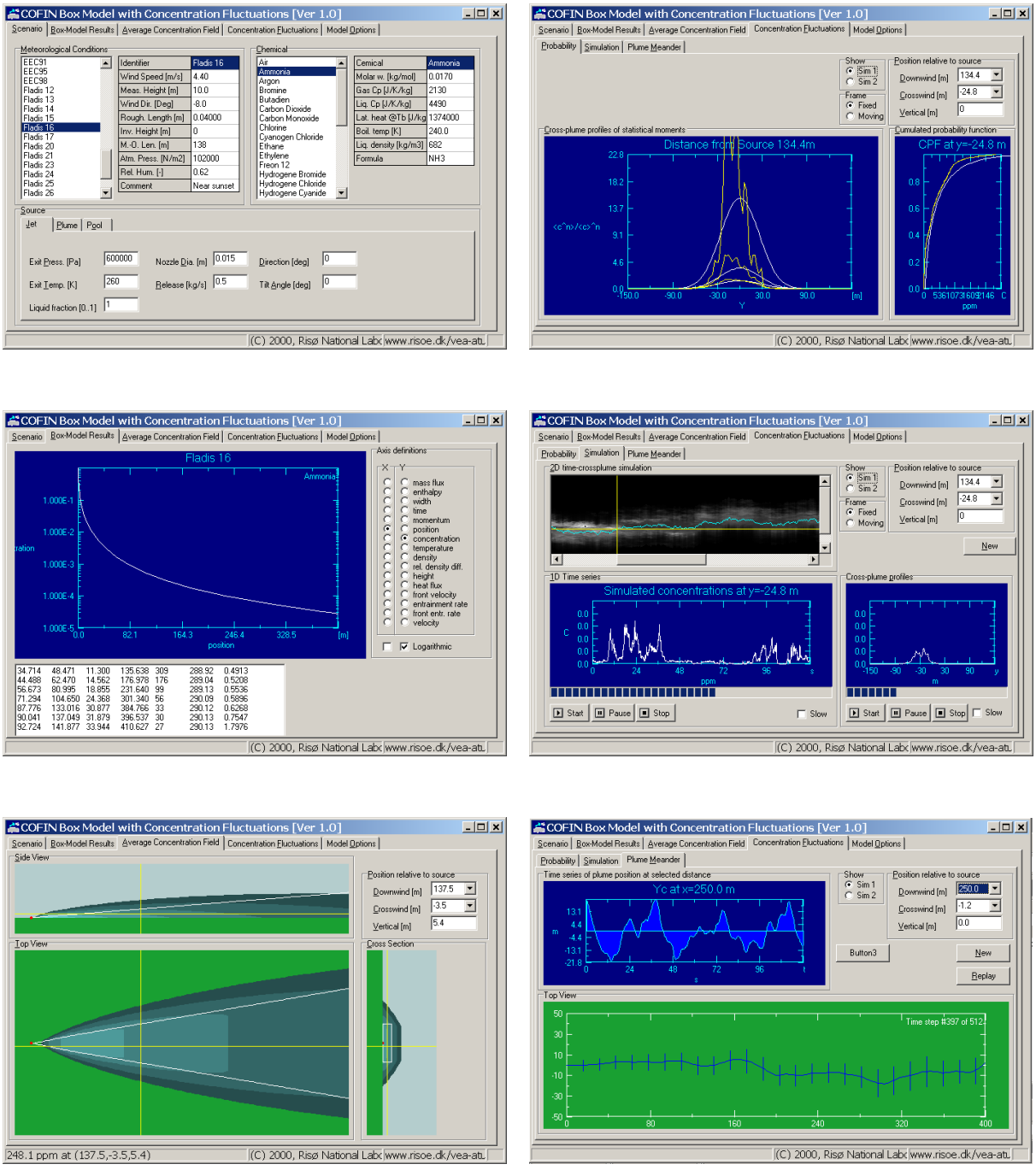

Figure 17. Screen dumps from the COFINBOX user interface. On the left-hand side: 1) Meteorology, substance properties and source models, 2) results of the box-model calculation, 3) contour plots. Modules for concentration fluctuations are shown on the right-hand side: 1) profiles of statistical moments and probability distributions, 2) Simulated concentration fluctuations, 3) Simulated plume meander.

eddies longer that those of small eddies. At each time step a gaussian puff is released from the source. The time-varying stochastic wind field transports the puff while its dimension increases and it is split into smaller ones when it has grown to a predefined size. Finally, instantaneous concentration fields are interpreted as the superposition of all puffs in the domain using cubic-spline interpolation along traces of puffs. Spatial moments of the concentration field are calculated as a function of distance from the source, and this leads to time series for the centre-line position and plume width.

Figure 17 shows the COFINBOX user interface.

Dissemination of results

publications

In addition to the present report the project published: five journal papers (Munro, Chatwin & Mole 2001b, Chatwin & Mole 2000, Mole 2001, Chatwin 2001, Munro, Chatwin & Mole 2001a); four encyclopedia articles (Nielsen 2001, Nielsen 2002, Chatwin & Sullivan 2001, Chatwin & Sullivan 2002); a Ph.D. thesis (Munro 2001); a data report (Jørgensen & Nielsen 1999); and eighteen conference papers, see homepage. The project has material for more publications, where the sponsorship will be acknowledged.

workshop

A workshop called *Fluctuations in Atmospheric Dispersion and their Applications (FADA)*, was arranged at the University of Sheffield, 9-12 September 2000. The FADA workshop had approximately 40 participants from four continents, with three panel discussions and 25 presentations, including eight presentations by COFIN participants. Potential model were invited to project meetings and to the FADA workshop. User needs were discussed Shell Research (UK), Health and Safety Executive (UK) and with scientific collaborators from the University of Western Ontario (Canada); the University of Alberta (Canada); Mitsubishi Heavy Industries (Japan); Defence Evaluation and Research Agency (UK) and Meteorological Office (UK). Scientist from these institutions visited Risø and Sheffield University on several occasions.

collaboration

homepage

The project homepage *http://www.risoe.dk/vea-atu/cofin* was active from the start of the project and it contains links and references to all management and scientific documents. The user-friendly COFINBOX program is available from here.

Contact

scientific staff

Participants of the COFIN project are reached at the following coordinates:

Scientist	Tel. No.	E-mail
Philip Chatwin	+44.114.2223740	P.Chatwin@sheffield.ac.uk
Hans E. Jørgensen	+45.46.775034	Hans.E.Joergensen@risoe.dk
Nils Mole	+44.114.2223772	N.Mole@sheffield.ac.uk
Rick Munro	+44.122.3337846	R.J.Munro@damtp.cam.ac.uk
Morten Nielsen	+45.46.775022	N.M.Nielsen @risoe.dk
Søren Ott	+45.46.775111	Soeren.Ott @risoe.dk

and the addresses are

Coordinator	Contractor
Risø National Laboratory	Sheffield University
Wind Energy Department	School of Mathematics and Statistics
Attn: Morten Nielsen	Attn: Prof. P.C. Chatwin
Building 125	The Hicks Building
P.O.Box 49	P.O.Box 597
DK-4000 Roskilde	Sheffield S10 2UN
Denmark	Great Britain
Fax:+45.46.775970	Fax: +44.114.2223739

The COFIN project collaborated with parallel research at *collaboration*

- The University of Western Ontario, London, Canada (Canada)
- The University of Alberta (Canada)
- Mitsubishi Heavy Industries (Japan)
- Defence Evaluation and Research Agency (UK)
- Meteorological Office (UK)

Scientist from these institutes visited the COFIN partners on several occasions and participated in the FADA workshop.

References

Chatwin, P. C. (2001). Some remarks on modelling the PDF of the concentration of a dispersing scalar in turbulence, *Euro. J. Appl. Math.*

Chatwin, P. C. & Mole, N. (2000). Evaluation of statistical models in atmospheric dispersion modelling, *Int. J. Environ. Poll.*, **14**, 106–114.

Chatwin, P. C. & Sullivan, P. J. (2001). Contaminant concentration fluctuations, *in* M. Fingas (ed.), *The handbook of hazarduous materials spill technology*, McGraw-Hill, NY, 25.1–16.

Chatwin, P. C. & Sullivan, P. J. (2002). Turbulent diffusion, *in* A. H. El-Shaarawi & W. W. Piegorsch (eds), *Encyclopedia of Environmetrics*, John Wiley & Sons.

Gioffrè, M., Gusella, V. & Grigoriu, M. (2000). Simulation of non-Gaussian field applied to wind pressure fluctuations, *Prob. Engn. Mech.*, **15**, 309–389.

Jørgensen, H. E. & Nielsen, M. (1999). Lidar data used in the COFIN project, *Risø-R-1127(EN)*, Risø National Laboratory.

Mole, N. (2001). The large time behaviour in a model for concentration fluctuations in turbulent dispersion, *Atmos. Environ.*, **35**, 833–844.

Munro, R., Chatwin, P. C. & Mole, N. (2001a). A concentration PDF for the relative dispersion of a contaminant plume in the atmosphere, *Boundary-Layer Meteorol.* Submitted.

Munro, R., Chatwin, P. C. & Mole, N. (2001b). The high concentration tails of the PDF of a dispersing scalar in the atmosphere, *Boundary-Layer Meteorol.*

Munro, R. J. (2001). *Models for Concentration Fluctuations in Relative and Absolute Dispersion*, Ph. D. Thesis, University of Sheffield.

Nielsen, M. (2001). Spreading of cold dense clouds, *in* M. Fingas (ed.), *The handbook of hazarduous materials spill technology*, McGraw-Hill, NY, 18.1–16.

Nielsen, M. (2002). Atmospheric dispersion: Heavy gases, *in* A. H. El-Shaarawi & W. W. Piegorsch (eds), *Encyclopedia of Environmetrics*, John Wiley & Sons, 125–130.

Press, W. H., Flannery, B. P., Teukolsky, S. A. & Vetterling, W. T. (1992). *Numerical Recipes in C, second edition*, Cambridge University Press.